Journal of Theoretical and Applied Information Technology
31st May 2013. Vol. 51 No.3

ISSN: 1992-8645 www.jatit.org E-ISSN: 1817-3195

STEADY-STATE OF NUMERICAL MODEL AND THE DESIGN OF A WIDEBAND SEMICONDUCTOR OPTICAL AMPLIFIER USING THE FINITE DIFFERENCE METHOD

[1]A. ELYAMANI, [2]A. ZATNI, [3]A. ELKAAOUACHI, [4]A. MOUMEN, [5]H. BOUSSETA.

[1,4,5]PhD Student, M.S.I.T Laboratory, Department of Computer Engineering high school of technology, Ibn Zohr University Agadir Morocco.
[2]Prof., Department of Computer Engineering, high school of technology, Agadir Morocco
[3]Prof., Department of physics, faculty of sciences, Ibn Zohr university Agadir Morocco
E-mail: [1]abdenbi.elyamani@gmail.com

ABSTRACT

The design of a semiconductor component such as semiconductor optical amplifiers (SOAs) necessarily needs to go through a phase of modeling which allows studying a theoretical characterization of the SOA and anticipating its reactions on the basis of the operating conditions. This will ensure a qualitative prediction of most accurate performance of the SOA. The development of a theoretical model is a multidisciplinary activity that needs engineering skills, optimization and physics. In this paper, we propose a numerical algorithm which enables the efficient implementation of the model, by the means of the finite difference method (FDM) and the rate equations. The model can be used to investigate the effects of different material and geometrical parameters on SOA characteristics. It is found that at low input optical power, the carrier density has a symmetrical spatial distribution, while at high input optical power, the carrier density spatial distribution becomes more asymmetrical. For input optical powers less than -25 dBm, the gain of the amplifier remains constant for different values of the molar fraction of arsenide and it reaches the maximum when y = 0.892. In our study, among the aspects of the importance of SOA is the use of an electrical controlled optical gate when the cavity lengths are great and the values of the molar fraction of arsenide are low. Using this model, our simulation results go in accordance with some published results for SOAs.

Keywords: *Semiconductor optical amplifier (SOA), Modeling, Finite difference method (FDM).*

1. INTRODUCTION

Semiconductor Optical Amplifiers (SOAs) are expected to become key elements in optoelectronic integrated systems and fiber transmission systems [1]-[2]. The SOAs have great potential as in-line optical amplifier for WDM systems due to their advantages of simple structure and ease of integration with other optical functional devices such as DFB and DBR [3]-[4]-[5]. The SOAs characteristics of wide bandwidth, high-saturation output power are needed for WDM application for the sake of covering more channels and reducing the signal crosstalk caused by the short carrier lifetime of SOAs. Mathematical models are required to aid in the design of SOAs and to predict their operational characteristics.

The theoretical foundation of SOAs modeling was established in 1980s [6]. Since then, major progress concerning SOA modeling start to focus on the material gain coefficient, spontaneous emission rate and the fraction of spontaneous emissions coupled with the guided waves in an amplifier. Some numerical simulations which use the Finite Difference Method (FDM) have been studied intensively to solve carrier rate equation and photon traveling wave equations.

FDM is the method that is the most to solve the Ordinary Differential Equations (ODEs) and the Partial Differential Equations (PDEs) in a bounded domain. The basic idea of finite difference methods is simple: derivatives in differential equations are written in terms of discrete quantities of dependent and independent variables, resulting in simultaneous algebraic equations with all unknowns prescribed at discrete nodal points of the entire domain. Briefly, the different unknowns when applying FDM are defined by their values on discrete (finite) grid and differential operators are replaced by difference operators using neighboring points [7]. We propose a numerical model to determine the steady-state properties of SOA over a

Journal of Theoretical and Applied Information Technology
31st May 2013. Vol. 51 No.3

ISSN: 1992-8645 www.jatit.org E-ISSN: 1817-3195

wide range of operating regimes [8]. In this model, a new gain coefficient model of bulk $InGaAsP$ SOAs developed by Connelly is applied, which includes the internal loss variation with the electron carrier density.

In this paper, we have developed a different numerical algorithm in more details on the basis of many studies and surveys done by [6]-[8]-[9]. Accordingly, we have programmed this numerical algorithm using Language C++ so as to undertake a study on the effect of the change of set parameters on the carrier density, the refractive index and the gain of the amplifier of a bulk InP-$InGaAsP$ homogenous buried ridge stripe SOA. These parameters are the input signal power, the bias current, the molar fraction of arsenide, the length of the cavity SOA and the temperature. The results we have gained provide an instructive insight about SOA, and they are also beneficial for device design and optimization.

2. THEORY OF SOA.

2.1 Material Gain Coefficients.

The Semiconductor Optical Amplifier (SOA) modelled is a 1.55 µm $InP-In_{1-x}Ga_xAs_yP_{1-y}$ homogeneous buried ridge stripe device. x and y are the molar fractions of Gallium and Arsenide, respectively in the undoped active region. Lattice matching is assumed, for which $x = 0.47y$ [8]. The model allows one to calculate the stimulated emission and stimulated absorption coefficients, from which the material gain coefficient is obtained as [8].

$$g_{m(\vartheta,n)} = \frac{C^2}{4\sqrt{2}\pi^{3/2} n_r^2 \tau_{rad} \vartheta^2} \left(\frac{2m_e m_{hh}}{\hbar\ (m_e+m_{hh})}\right)^{3/2} \times \sqrt{\vartheta - \frac{E_g(n)}{h}} \left(f_c(\vartheta) - f_v(\vartheta)\right) \quad (1)$$

Whereas C is the speed of light in vacuum, ϑ optical frequency, n_r the active region refractive index, τ_{rad} the radiative carrier recombination lifetime and $\hbar$ Planck's constant h divided by 2π.

TABLE I: SOA GEOMETRICAL AND MATERIAL PARAMETERS [8]:

Symbol	Parameters	Value
y	Molar fraction of Arsenide in the active region.	0.892
L	Cavity length	700 μm
d	Active region thickness	0.4 μm
W	Central active region width	0.4 μm
K_g	Bandgap shrinkage coefficient	$0.9 \times 10^{-10} eVm$
n_{eq0}	Equivalent refractive index at zero carrier density.	3.22
$\frac{dn_{eq}}{dn}$	Differential of equivalent refractive index with respect to carrier density.	$-1.34 \times 10^{-26} m^{-3}$
Γ	Optical confinement factor	0.45
η_{in}	Input coupling loss.	3.0 dB
η_{out}	Output coupling loss.	3.0 dB
R_1	Input facet reflectivity	5×10^{-5}
R_2	Ouput facet reflectivity	5×10^{-5}
K_0	Carrier independent absorption loss coefficient	6200 m^{-1}
K_1	Carrier dependent absorption loss coefficient	$7500 \times 10^{-24}\ m^2$
A_{rad}	Linear radiative recombination coefficient	$1 \times 10^7\ s^{-1}$
B_{rad}	Bimolecular radiative recombination coefficient	$5.6 \times 10^{-16} m^3\ s^{-1}$
A_{nrad}	Linear nonradiative recombination coefficient due to traps	$3.5 \times 10^8\ s^{-1}$
B_{nrad}	Bimolecular nonradiative recombination coefficient	$0.0 \times 10^{-16} m^3\ s^{-1}$
C_{aug}	Auger recombination coefficient	$3.0 \times 10^{-41} m^6\ s^{-1}$
D_{leak}	Leakage recombination coefficient	$0.0 \times 10^{48} m^{13.5}\ s^{-1}$
a	Bandgap energy quadratic coefficient	1.35
b	Bandgap energy quadratic coefficient	−0.775
c	Bandgap energy quadratic coefficient	0.149
m_e	Effective mass of electron in the CB	$4.10 \times 10^{-32}\ kg$
m_{hh}	Effective mass of heavy hole in the VB	$4.19 \times 10^{-31}\ kg$
m_{lh}	Effective mass of light hole in the VB	$5.06 \times 10^{-32}\ kg$

m_e and m_{hh} are the conduction band (CB) electron and valence band (VB) heavy hole effective masses, respectively. n is the CB carrier (electron) density. $f_c(\vartheta)$ and $f_v(\vartheta)$ are the occupation probability of an electron with frequency ϑ in the CB and an electron with frequency ϑ in VB, respectively. The bandgap energy E_g can be expressed as [8].

$$E_g(n) = E_{g0} - \Delta E_g(n) \quad (2)$$

E_{g0} , the bandgap energy with no injected carriers is given by the quadratic approximation .

$$E_{g0} = e(a + b.y + c.y^2) \quad (3)$$

Whereas a, b and c are the quadratic coefficients and e is the electronic charge. $\Delta Eg(n)$ is the bandgap shrinkage due to the injected carrier density given by [6].

$$\Delta E_g(n) = e.K_g n^{1/3} \quad (4)$$

Whereas Kg is the bandgap shrinkage coefficient.

The equation (1) can be decomposed into two components: a gain coefficient, g'_m and absorption coefficient, g''_m, so

$$g_m(\vartheta,n) = g'_m(\vartheta,n) - g''_m(\vartheta,n) \quad (5)$$

Whereas g'_m and g''_m are defined by equations (16) and (17) of [8].

Journal of Theoretical and Applied Information Technology
31st May 2013. Vol. 51 No.3

ISSN: 1992-8645 www.jatit.org E-ISSN: 1817-3195

Fig. 1 shows the material gain coefficient, stimulated gain and absorption gain coefficients, g_m, g'_m and g''_m respectively, as a function of signal wavelength in the range of $1.30\,\mu m$ to $1.65\,\mu m$ for $InP - In_{1-x}Ga_xAs_yP_{1-y}$ at arsenide molar fraction, $y = 0.892$.

Our calculations were performed at room temperature (300K) and carrier density of the active region, $n = 2.10^{24}\,m^{-3}$. The value of the maximum gain coefficient was observed among the wavelength $1540\,nm$.

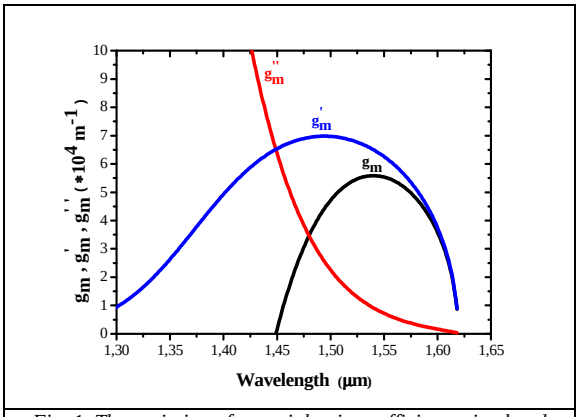

Fig. 1. The variation of material gain coefficient, stimulated gain and absorption gain coefficients with wavelength at room temperature (27 ℃)

In addition to the intrinsic material absorption, light propagating in an SOA is subject to a number of additional loss mechanisms. The total loss coefficient of an SOA active region can be modelled by [10]:

$$\alpha(n) = K_0 + \Gamma K_1 n \quad (6)$$

Whereas K_0 and K_1 are the carrier independent and carrier dependent absorption loss coefficients respectively. K_0 represents the intrinsic material and waveguide losses. K_1 is mainly due to intervalence band absorption and carrier dependent scattering losses. The net gain coefficient g_n of an SOA is then given by [10]:

$$g_n(\vartheta, n) = \Gamma g_m(\vartheta, n) - \alpha(n) \quad (7)$$

2.2 System Equations of SOA.

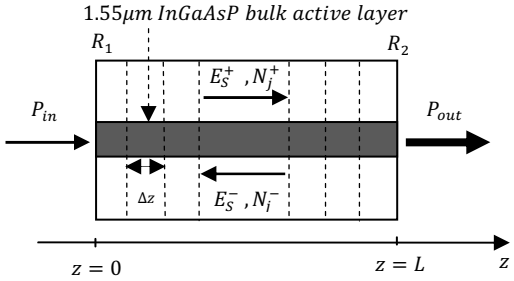

Fig. 2 Schematic view of a typical SOA structure. The number of subsections discretized in the wave propagation direction is $N_z = 70$ sections.

Fig. 2 shows the schematics of SOA, in left (input) and right (output) facets have power reflectivities R_1 , and R_2, respectively. The signal wave get partially transmitted and reflected from the two facets of the amplifier. As result, the signal wave is amplified in two directions, forward direction and backward direction, and there are two sets of traveling waves originated from the signal. In the amplifier, the spatially varying component of the field due to the input signal can be decomposed of two complex traveling-waves: E_s^+ and E_s^- propagating in the positive and negative z directions respectively which obey the following complex differential equations [8]:

$$\begin{cases} \frac{dE_S^+(z)}{dz} = \left(-j\beta(n) + \frac{1}{2}g_n(\vartheta, n)\right)E_S^+(z) & (8) \\ \frac{dE_S^-(z)}{dz} = \left(+j\beta(n) - \frac{1}{2}g_n(\vartheta, n)\right)E_S^-(z) & (9) \end{cases}$$

Whereas $j = \sqrt{-1}$ and β is a propagation constant for this signal frequency ϑ.

$$\beta(n) = \frac{2\pi n_{eq}(n)\vartheta}{c} \quad (10)$$

$n_{eq}(n)$ is the equivalent refractive index of the active region of the SOA.

$$n_{eq}(n) = n_{eq0} + \frac{dn_{eq}}{dn}n \quad (11)$$

n_{eq0} is the equivalent refractive index with no pumping, $\frac{dn_{eq}}{dn}$ is the differential of equivalent refractive index. It is assumed that the modulus squared of the amplitude of the traveling-wave is equal to the photon rate of the wave in that direction, so:

$$N_S^+ = |E_S^+|^2 \quad \text{and} \quad N_S^- = |E_S^-|^2 \quad (12)$$

These amplified forward and backward signal waves should meet the following boundary conditions:

Journal of Theoretical and Applied Information Technology
31st May 2013. Vol. 51 No.3

ISSN: 1992-8645 www.jatit.org E-ISSN: 1817-3195

$$E_s^+(0) = \left(1 - \sqrt{R_1}\right)E_{in} + \sqrt{R_1}E_s^-(0) \quad (13)$$

$$E_S^-(L) = \sqrt{R_2}E_s^+(L)$$

Whereas E_{in} is the input signal field. it is defined by equation (23) of [8].

The SOA model is based on a set of coupled differential equations that describe the interaction between the internal variables of the amplifier, i.e., the carrier density and photon rates. The solution of these equations enables one to determine external parameters of SOA such as signal fiber-to-fiber gain and mean noise output to be predicted [8].

On the other hand, N_j^+ and N_j^- are defined as the spontaneous emission photon rates for a particular polarization in a frequency spacing $K_m\Delta\vartheta_m$ centred on frequency ϑ_j travelling in the positive and negative z directions, respectively. This is defined by equation (31) of [6], K_m is a positive integer, and $\Delta\vartheta_m$ is the longitudinal mode frequency spacing described by equation (33) of [8]. Those spontaneous emission photon rates are observed in the following equation [8]-[11].

$$\begin{cases} \frac{dN_j^+(z)}{dz} = +g_n(\vartheta, n)N_j^+(z) + R_{sp}(\vartheta_j, n) & (14) \\ \frac{dN_j^-(z)}{dz} = -g_n(\vartheta, n)N_j^-(z) - R_{sp}(\vartheta_j, n) & (15) \end{cases}$$

Subject to the boundary conditions

$$N_j^+(0) = R_1N_j^-(0)\,;\;\; N_j^-(L) = R_2N_j^+(L) \quad (16)$$

Whereas $R_{sp}(\vartheta_j, n)$ represents the spontaneously emitted noise coupled into N_j^+ or N_j^-.

2.3 Carrier-Density Rate Equation.

The carrier density at position z in the amplifier obeys the rate equation [8]:

$$\frac{dn(z)}{dt} = \frac{I}{edLW} - R(n(z)) \quad (17)$$
$$- \frac{\Gamma}{dW}\left\{\sum_{k=1}^{N_s} g_m(\vartheta_k, n(z))[N_{sk}^+(z) + N_{sk}^-(z)]\right\}$$
$$- \frac{2\Gamma}{dW}\left\{\sum_{j=0}^{N_m-1} g_m\left(\vartheta_j, n(z)\right)\left[N_j^+(z) + N_j^-(z)\right]\right\}$$

Whereas I is the amplifier bias current, d and W are the active region thickness and width, respectively. The first term on the Right Hand Side (RHS) of (17) represents the addition of carriers to the active region from the bias current. These injected carriers are then depleted by various mechanisms occurring within the amplifier. The second term is due to radiative and nonradiative recombination mechanisms. The third and fourth terms represent radiative recombination of carriers due to amplified signal and ASE. The factor of two in (17) accounts of the fact that spontaneously emitted photons can exist in one of two mutually orthogonal polarizations (TE or TM).

The recombination rate term $R(n)$ is given by:

$$R(n) = R_{rad}(n) + R_{nrad}(n) \quad (18)$$

Whereas $R_{rad}(n)$ and $R_{nrad}(n)$ are the radiative and nonradiative carrier recombination rates, respectively, they are defined by equations (50) and (51) of [8].

SOA geometrical and material parameters used in the steady-state model are given in table I [8].

3. STEADY-STATE OF NUMERICAL ALGORITHM.

To solve the SOA equation numerically, the amplifier is divided into a number of sections labeled from $i = 1$ to Nz as shown in Fig. 2. The carrier rate equation and traveling wave equations for signal and spontaneous emission are estimated at the section interfaces. In the steady-state $\frac{dn}{dt}$ is zero. To predict the steady-state characteristics, an algorithm is used to adjust the carrier density so the value of $\frac{dn}{dt}$ throughout the amplifier approaches zero. A flowchart of the algorithm is shown in Fig.3. An initial guess value is used for the carrier density to calculate the forward and backward signals and the ASE propagation photon density along the device.

Multiple iterations are generally required to reach convergence. Detailed operating procedures for this numerical algorithm are listed as follows:

Step 1: Initialize the signal fields and spontaneous emission photon rates to zero, and obtain the initial carrier density from the solution of (17), with all fields set to zero, using the Newton-Raphson technique [12].

Step 2: Begin iteration and define the boundary conditions.

Journal of Theoretical and Applied Information Technology
31st May 2013. Vol. 51 No.3

ISSN: 1992-8645 www.jatit.org E-ISSN: 1817-3195

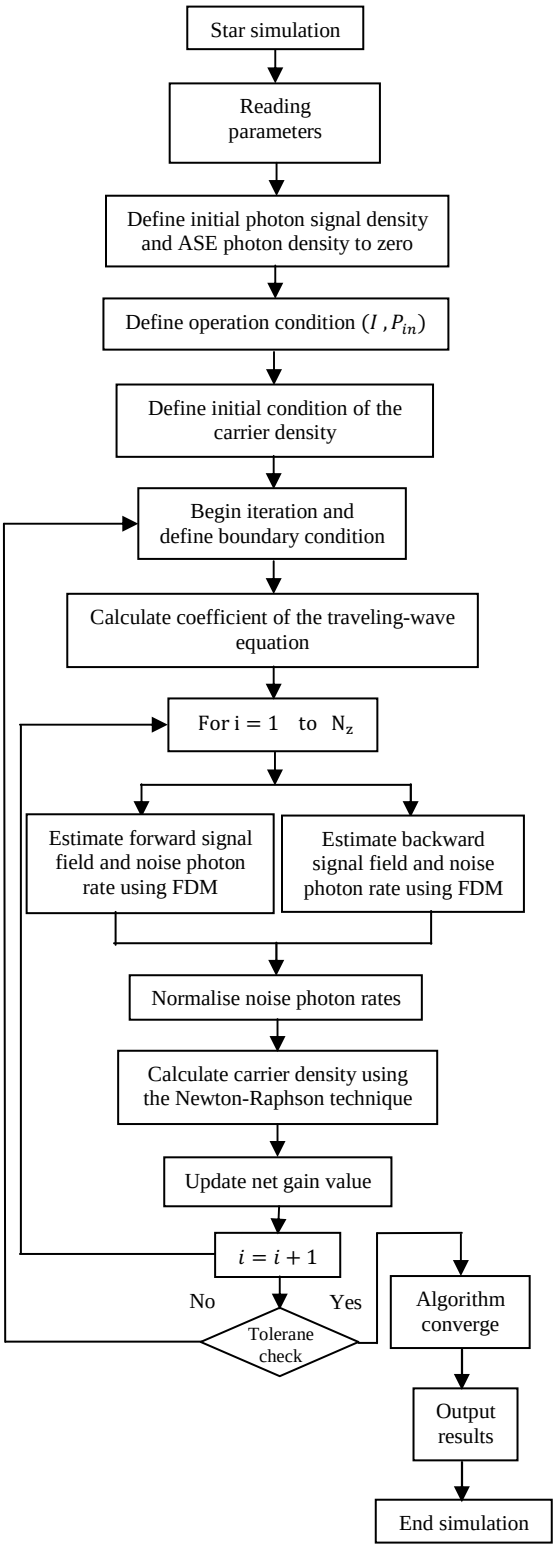

Fig. 3: Flowchart of SOA numerical model [6]-[8]-[9].

Step 3: Traveling-wave equations for signal and spontaneous emissions are estimated using finite difference solutions of (8)-(9) and (14)-(15) [8].
Step 4: The signal and spontaneous emissions results for each section from **Step 3** are applied to the carrier rate equation.

Step 5: The carrier density for each section is calculated using the Newton-Raphson technique.
Step 6: Check the carrier difference of the last iteration. If the differences of all sections are less than a predefined small value, a converged solution is achieved. Otherwise, go back to **step 2** to start a new iteration.

The algorithm was implemented using the program Language C++, for the sake of the usability and timeliness of execution.

4. RESULTS AND DISCUSION

In order to understand the input power effect, we have plotted in Fig. 4 the carrier density longitudinal distribution, the refractive index longitudinal distribution, the forward and backward ASE photon rates, and the forward signal photon rates longitudinal distributions for two different injected signal powers, -40 and -10 dBm. These simulated results go in accordance with some published results [8]. At low input optical power, the carrier density has a symmetrical shape with a peak at the centre of the SOA (Fig. 4-(a)). In fact, the forward and backward travelling of ASE signals are respectively maximum at the output and input facets deplete the carrier density in these regions (Fig. 4-(c)). The signal photon rate grows along the propagation axis and starts to become significant after $\left(z = \frac{L}{2}\right)$ (Fig. 4-(e)). At high input optical power, the carrier density becomes asymmetrical and the peak is shifted to the input facet (Fig. 4-(b)).This phenomenon can be explained by the signal propagation dominance. The signal photon rate starts to grow significantly at $\left(z = \frac{L}{7}\right)$ but saturates at the output facet of the device due to the strong carrier depletion (Fig. 4-(f)). From the equation (12) the refractive index varies inversely with the carrier density (Fig. 4-(a)-(b)).

The carrier consumption and the saturation effects become more important at high input electrical injection (Fig. 5 and 6).

ISSN: 1992-8645 www.jatit.org E-ISSN: 1817-3195

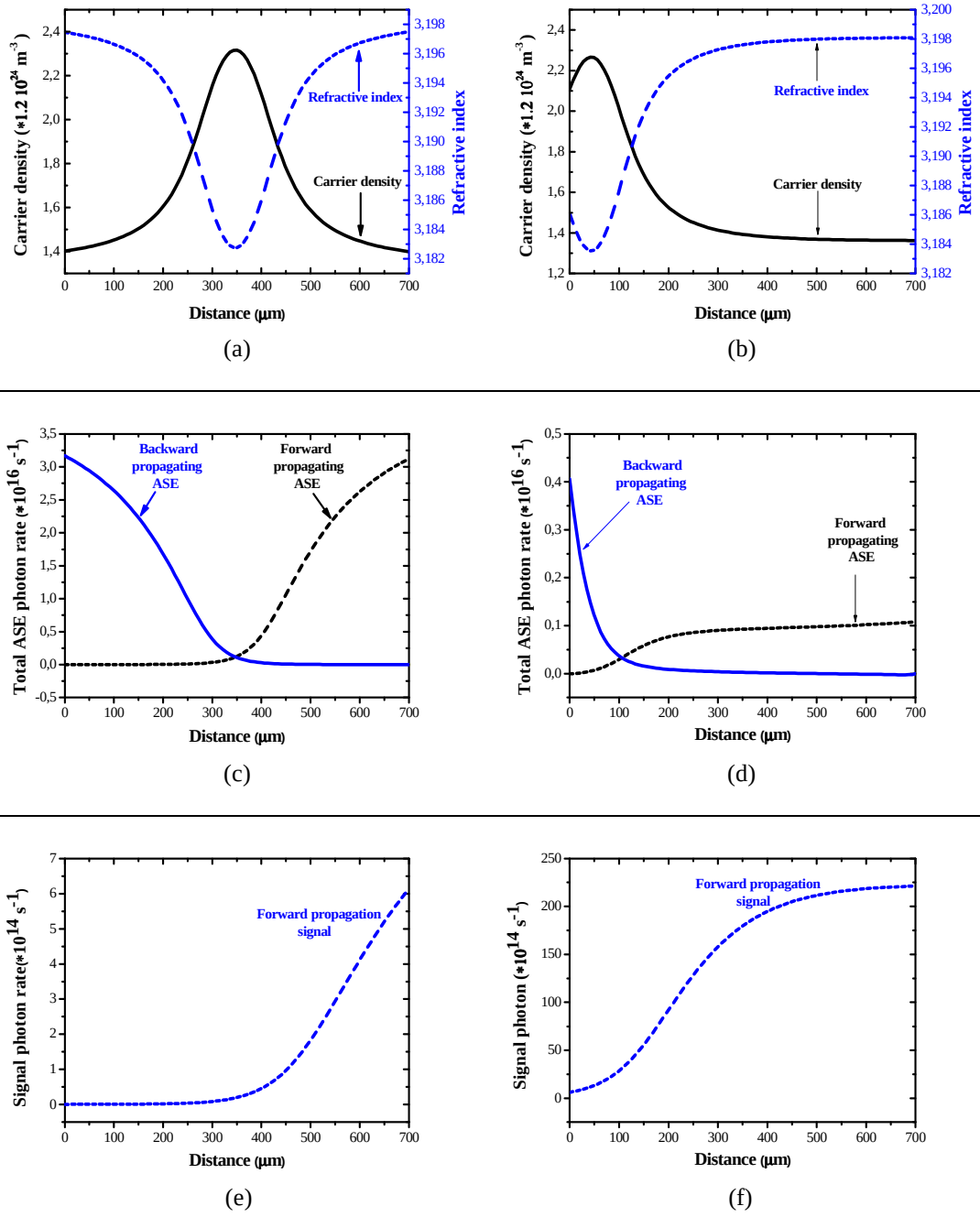

Fig. 4: Carrier density, forward and backward propagating total ASE photon rates and signal photon rates spatial distributions.(a), (c) and (e) represents the simulation for $P_{in} = -40\ dBm$; (b), (d) and (f) for $P_{in} = -10\ dBm$. Signal wavelength is 1.54 μm and the bias current is 130 mA. The device parameters are as in Table I.

ISSN: 1992-8645 www.jatit.org E-ISSN: 1817-3195

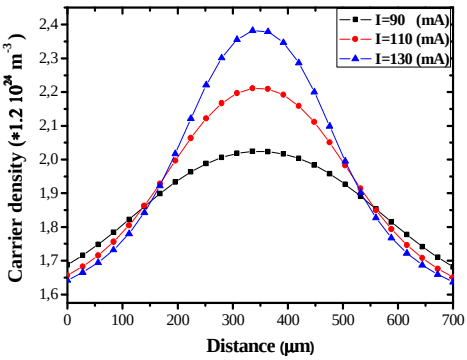

Fig. 5: Carrier density spatial distribution along the active region of the SOA at different bias current. The input signal has a Signal wavelength is 1.54 *μm and power of -40dBm.*

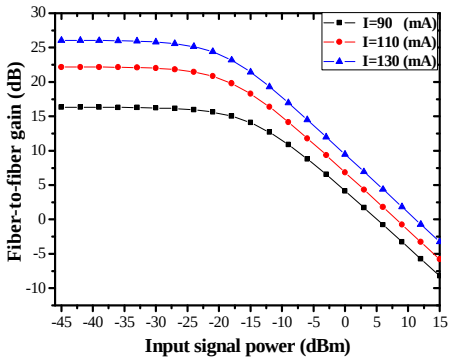

Fig. 6: SOA fiber-to-fiber gain versus input signal power at different bias current. Signal wavelength is 1.54 *μm .*

The variation of the semiconductor molar fractions leads to a different compound with new material parameters. The effect of increasing the molar fraction of arsenide slightly decreases the carrier density especially at the end facets of the SOA because when increasing molar fraction of arsenide in the *InGaAsP* active region, the forward and backward ASE photon rates at the end facets of the amplifier -shown in [13]-[14]- become larger that lead to a large consumption of free carriers in the CB.

However, the effect of changing the molar fraction of arsenide is significant in the distribution of forward and backward signal photon rates along the active region of the SOA as shown in Fig.7. It is obvious that the forward and backward signal photon rates have a maximum value at end facets of the SOA when the arsenide molar fraction equals 0.892.

Fig.8 depicts the simulated amplifier fiber-to-fiber gain versus input signal power at different values of the molar fraction of arsenide. In this Figure, it is evident that when the input signal power is less than $-25\ dBm$, the gain of the amplifier remains constant for each value of y (molar fraction of arsenide), and it reaches the maximum when the molar fraction of arsenide is equal to 0.892. Any increase or decrease of this value will lessen the maximum value of signal photon rates at the end facets and even lessen the gain of the SOA for power optical input below $-25\ dBm$. This is due to the best lattice matching between the cladding and active region substrates occurring at y=0.892.

Fig.9 shows the simulated carrier density distribution versus the position along the active region at different values of temperatures.

The amplifier fiber-to-fiber gain versus input signal power at different values of temperatures is shown in Fig.10.

It is obvious that there is an increased probability of breaking covalent bonds when the temperature increases, which leads to the liberation the electrons [14].

It can be seen that when the temperature increases, the evolution of the carrier density becomes high (Fig.9) but that evolution does not appear for the gain of the amplifier that decreases with temperature (Fig.10). All this is due to the increase of absorption rate with increasing temperature which minimizes the number of carriers available for participating in the process of stimulated emission.

Journal of Theoretical and Applied Information Technology
31st May 2013. Vol. 51 No.3

ISSN: 1992-8645 www.jatit.org E-ISSN: 1817-3195

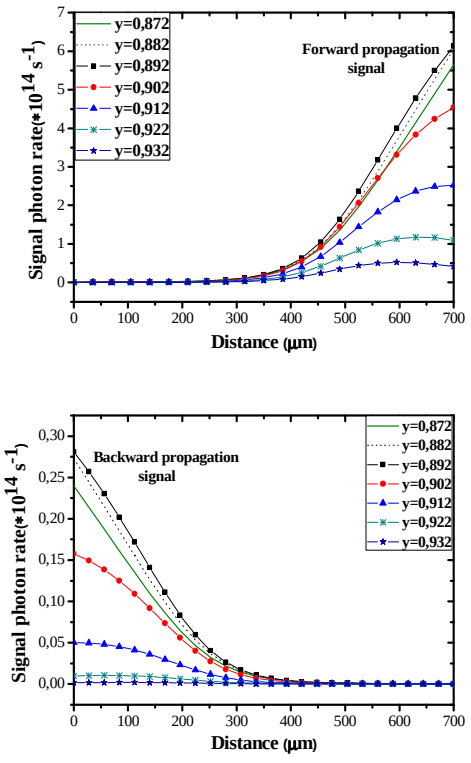

Fig. 7: Forward and Backward propagating signal photon rates spatial distribution along the active region of the SOA at different values of the molar fraction of arsenide . $P_{in} = -40\ dBm$.

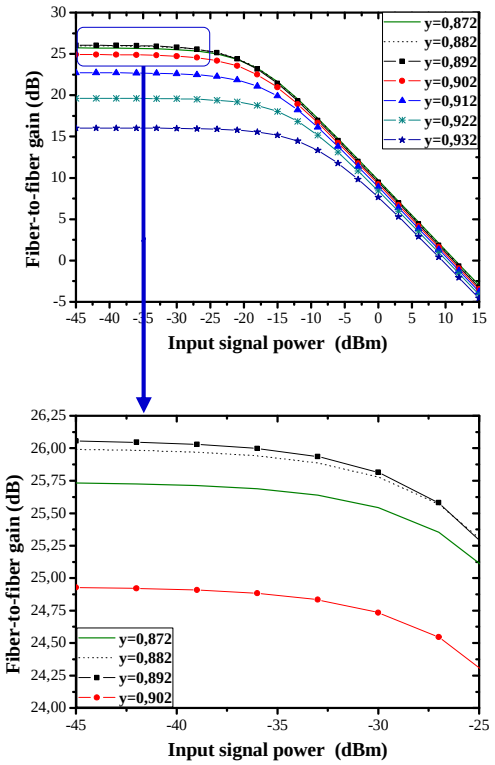

Fig. 8: SOA output signal power versus input signal power at different values of the molar fraction of arsenide. Signal wavelength is 1.54 μm and bias current is 130 mA.

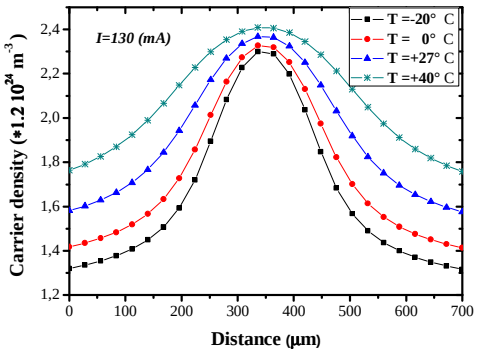

Fig. 9: Carrier density spatial distribution along the active region of the SOA at different temperatures. The input signal has a Signal wavelength is 1.54 μm and power of -40dBm.

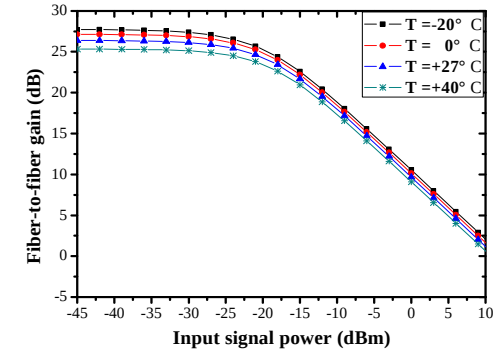

Fig. 10: SOA fibe r-to-fiber gain versus input signal power at different temperatures. Signal wavelength is 1.54 μm and bias current is 130 mA.

ISSN: 1992-8645 www.jatit.org E-ISSN: 1817-3195

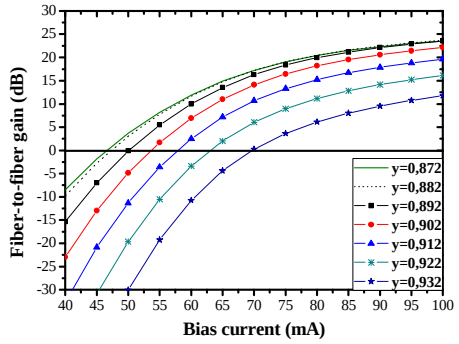

Fig. 11: SOA fiber-to-fiber gain versus bias current at different values of arsenide molar fraction. The input signal has a Signal wavelength is 1.54 *µm and power of -30dBm..*

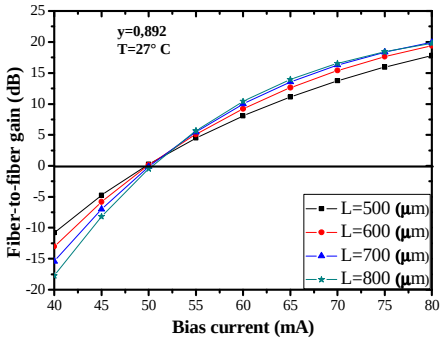

Fig. 12: SOA fiber-to-fiber gain versus input signal power at different values of the length of the cavity. The input signal has a Signal wavelength is 1.54 *µm and power of -30dBm..*

Another crucial point in the study of the amplification function is the relationship between the gain of the SOA and the bias current. According to Fig.11, it is interesting to note that the gain is unitary, i.e. (G = 0 dB) at some currents for each value of the molar fraction of arsenide: the intrinsic gain equals then the total loss. Below these currents, the SOA presents the loss that is mainly due to the absorption. According to Fig.12, there is a slight variation of the bias current I, that generates a significant increase in the gain of the amplifier. One can also notice that the slope of the curve increases remarkably with increasing length of the cavity of SOA, however, the volume remains constant.

Here, we can now take note of the importance of SOA for designing an electrically controlled optical gate. Since when the current changes within a short interval, we obtain a big variation in the gain of the amplifier and suddenly the extinction ratio becomes high. Especially, for great cavity lengths and low values of molar fraction of arsenide.

5. CONCLUSION

In this study, the SOA carrier density spatial variation, the gain of the amplifier, the forward and backward signal photon rates and the total ASE photon rates distributions are all studied under the effect of the change a set of parameters such as input signal power, bias current, molar fraction of arsenide, length of the cavity of SOA and temperature. In this piece works, among the aspects of the importance of SOA is the use of an electrical controlled optical gate when the cavity lengths are great and the values of the molar fraction of arsenide are low. To demonstrate the capability of the model, some simulation results of SOA were presented. The function of SOA in photonics will be analogy with ones of the functions in the electronics and that will be the subject of our future study.

REFRENCES:

[1] Agrawal, G.P, Fiber-Optic Communication Systems, Volume 1. 3rd Edn, Wiley-Interscience, New York, USA., ISBN-13: 9780471215714, 2002.

[2] Ronald W. Waynant (Author), Marwood N. Ediger (Editor), Ronald Waynant (Author), Electro-optics Handbook, Optical and Electro-Optical Engineering Series, 1st edition, 1994.

[3] A. Zatni and J. Le Bihan, "Analysis of FM and AM responses of a tunable three-electrode DBR laser diode," *IEEE Journal of Quantum Electronics*, vol. 31, pp. 1009-1014, 1995.

[4] A.Moumen, A. Zatni "a novel design of quarter wave-shifted distributed feedback semiconductor laser for high-power single-mode operation," *Journa of Theoretical and Applied Information technologie*, vol. 38, pp. 210-218, 2012.

[5] X.Li, J.Park,"Time-domain simulation of channel crosstalk and inter-modulation distortion in gain-clamped semiconductor optical amplifiers," *optics communications, vol. 263, pp. 219-228, 2006.*

ISSN: 1992-8645 www.jatit.org E-ISSN: 1817-3195

[6] Dong-Xue Wang, JOHN A.Buck, Kevin Brennan, and Ian Ferguson."A numerical model of wavelength converters based on cross-gain modulation in semiconductor optical amplifiers," *Applied Optics Engineer, vol. 45, pp.47014-4708, 2006.*

[7] K.W.Morton, and D.F.Mayers, Numerical Solution of Partial Differentiel Equations, Cambridge University Press, 2005.

[8] M.J.Connelly,"Wideband Semiconductor Optical Amplifier Steady-state Numerical Model," *IEEE J. Quantum Electron*, vol. 37, pp. 439-447, 2001.

[9] G. de Valicourt, F.Pommereau, F. Poingt, M. Lamponi, G.H.Duan, P.Chanclou, M.A.Violas and R.Brenot,"Chirp Reduction in Directly Modulated Multielectrode RSOA Devices in Passive Optical Networks ," *Photonics technology letters*, Vol. 22, pp.1425-1427, 2010

[10] Michael J.Connelly,"Semiconductor Optical Amplifiers," Boston, MA: Kluwer Academic Publishers, 2002.

[11] M. Menif, Student Member, IEEE, W. Mathlouthi, P. Lemieux, L. A. Rusch, Senior Member, IEEE , "Error-Free Transmission for Incoherent Broad-Band Optical communication Systems Using Incoherent-to-CoherentWavelength Conversion," *Journal of Lightwave Technology*, vol. 23, pp. 287-294, 2005.

[12] W.H.Press,B.P.Flannery,S.A.Teukolsky, and W.T.Vetterling, *Numerical Recipers in Pascal.* Cambridge, MA: Cambridge Univ.Press, 1994.

[13] O. Mahran, M.T.Al Absy, M.S.Helmy and G.D.Roston,"Carrier Density and Photon Rates Distributions of Active Region of a Wideband Semiconductor Optical Amplifiers," *Trends in Applied Sciences Research*, vol. 7, pp. 370-381, 2012.

[14] K. ALFARAMAWI, O. MAHRAN, W. EL SHIRBEENY S. ABBOUDY "Steady-state properties of the wideband semiconductor optical amplifier," *Optoelectronics and Advanced Materials-Rapid Communications*, vol. 1, pp. 571-575, 2007.

[15] A. Moumen, A. Zatni, A. Elkaaouachi, A. Elyamani , H. Bousseta. "Time-Domain Large Signal Investigation on Dynamic Responses of the GDCC Quarterly Wavelength Shifted Distributed Feedback Semiconductor Laser," *International Journal of Advanced Computer Science and Applications, pp 165-170 Vol. 3, No.9, 2012.*